Process-Property Relationship in Polylactic Acid Composites Reinforced by Iron Microparticles and 3D Printed by Fused Filament Fabrication

Rezgar Hasanzadeh[1,], Peyman Mihankhah[1], Taher Azdast[1,*], Mahdi Bodaghi[2] , Mahmoud Moradi[3]**

1- Department of Mechanical Engineering, Faculty of Engineering, Urmia University, Urmia, Iran

2- Department of Engineering, School of Science and Technology, Nottingham Trent University, Nottingham, NG11 8NS, UK

3- Faculty of Arts, Science and Technology, University of Northampton, Northampton NN1 5PH, UK

*t.azdast@urmia.ac.ir **re.hasanzadeh@urmia.ac.ir

Abstract

Polylactic acid (PLA) is the most widely used material in the Fused Filament Fabrication (FFF) technique, which is a biocompatible thermoplastic. However, PLA's usefulness is limited by its narrow processing window and relatively low mechanical properties. Therefore, PLA composites have been developed to enhance its properties for FFF printing. A key challenge in producing composite parts via this method is to find the correlation between the mechanical properties of the parts and the process parameters. This knowledge is essential for optimizing the printing process to achieve the desired mechanical properties for composite parts in industries such as aerospace, automotive, and medical, where high-performance composite materials are crucial. The ability to control and predict the mechanical properties of FFF-printed composite parts is critical for their successful integration into these industries. In this study, the effect of nozzle temperature (NT), printing speed (PS), and nominal porosity (POR) on the impact strength and specific impact strength of PLA/iron composites was examined using FFF. Response surface methodology (RSM)

was used to optimize the experimental design. The results revealed that POR had the most significant effect on the impact resistance data, while NT had the least effect. Reducing the POR led to improved impact resistance in the samples. Multi-objective optimization results showed that the lowest NT (190 °C), the lowest POR (30 %), and a PS of 50 mm/s were the optimal conditions for multiple objectives. RSM was also utilized to develop mathematical models of impact properties, focusing on varying NT, POR, and PS, which can be used to predict desired impact properties.

Highlights

- Nominal porosity has the most influence on the impact strength of PLA/iron composites.
- Optimum values were temperature of 190 °C, nominal porosity of 30%, and speed of 50 mm/s.
- RSM was effective in enhancing the mechanical properties of composite materials.
- RSM models provide a predictive tool for future FFF-printed composite parts.
- Maximum impact strength of 4.44 kJ/m^2 was achieved.

Keywords: 3D printing; Composites; Impact resistance; Thermoplastics; Mechanical properties

1. Introduction

Time is one of the most important factors during the engineering process, but accuracy is another that must be kept in mind at all times. Due to its technological advantages, cost-effectiveness, and time-saving capabilities, additive manufacturing (AM) has caught the eye of engineers [1-3]. A lot of AM technologies are available today, but fused filament fabrication (FFF) is very popular due to its simplicity and low investment cost [4, 5]. This method uses filaments as raw materials which play a crucial role in the efficiency of FFF. Using a heated nozzle, a thermoplastic filament passes

through the nozzle and is deposited layer by layer according to a predetermined pattern on the heat bed adopted [6]. The polylactic acid (PLA) is the most commonly used raw filament in the FFF-based 3D printing processes due to its many advantages, including its biodegradability and eco-friendliness, easy printing, low melting point, no fumes, and low cost. Due to some of its drawbacks, such as a small processing window and relatively low mechanical properties, its application in the FFF technique has faced some obstacles [7-9]. In order to reduce these restrictions on the use of PLA, there are various techniques that can be used, such as cross-linking, copolymerization, and blending. In polymer blending, physical modifications are made to produce novel properties. Hence, to improve the properties of PLA printed by the FFF, researchers recommend preparing PLA composites with suitable additives [10]. A number of studies have been conducted on the development of chemical, physical and mechanical properties of PLA composite parts with filler materials such as aluminum (Al), bronze, copper (Cu), minerals, natural fibers, printed using FFF technology [11]. In one of these researches, Kottasamy et al. [12] examined the effect of different infill pattern on mechanical properties of PLA/Cu printed samples with varying Cu compositions (25 and 80 wt.%). Both Cu contents showed significant differences in all mechanical properties. Samples with 25 wt.% Cu and concentric infill pattern had the highest ultimate tensile strength and flexural strength, and samples with 25 wt.% Cu and grid infill pattern had the highest compressive strength. Similarly, Zhang et al. [13] printed pure PLA and Cu fiber reinforced-PLA composite specimens using FFF technique and compare their mechanical properties. A variety of raster angles were used to print the specimens (at 0°, 90°, 45°, 0°/90° and 0°/45°). The researchers found that the tensile strength of PLA/Cu composite specimens decreased with the addition of Cu fibers, while the elongation at break increased due to Cu fibers' higher elasticity and lower tensile strength. 0° raster angle PLA and PLA/Cu specimens had the highest

tensile strength, while 90° raster angle samples had the lowest. Additionally, they indicated that adding Cu fibers to PLA would improve its thermal stability. Liu et al. [14] focused on the mechanical properties of PLA composites based on ceramic, wood, carbon fiber and metal. For this purpose, they studied the effects of different PLA composites, build orientations and raster angles on the mechanical responses. It was demonstrated that ceramic, Al, and Cu-based PLA samples have similar or even enhanced mechanical properties when compared to pure PLA. The mechanical properties of pure PLA were significantly reduced when wood and chopped carbon fiber were added. Furthermore, the PLA composite samples printed in on-edge orientation with +45°/−45° raster angles exhibited the highest mechanical modulus and strength. In a study by Hanon et al. [15], the effect of the presence of bronze on tribological and mechanical properties of PLA/bronze composites was examined. Using bronze particles as reinforcement for PLA materials improved the tribological properties and had a significant impact on their mechanical properties. Also, their findings indicated that different print orientations have significant differences in the mechanical properties and tribological behavior of printed parts. Selvamani et al. [16] studied the tensile properties of PLA/brass composite at different infill patterns (octa-spiral, rectilinear, honeycomb, grid and concentric) and compositions (15 wt.% and 70 wt.%). In both combinations, the concentric pattern had the strongest and the octa-spiral pattern had the weakest properties in terms of elastic modulus, ultimate tensile strength, and yield strength. The mechanical characteristics of PLA with concentrations of 10 and 20 wt.% of Al powder were studied using FFF technique by Vinay et al. [17]. It was found that the hardness, ultimate tensile strength, yield strength increased and the percentage elongation decreased with the inclusion of Al powder. In addition to the tensile strength increased by 46%, the yield strength increased also by 84% after adding 20 wt.% Al to PLA. The ductility of PLA was also reduced as Al powder was incrementally

added. Patanwala et al. [18] evaluated the performance of carbon nanotubes-PLA (CNT/PLA) composite parts fabricated by the FFF method. In this study, PLA was compounded with 0.5, 2.5, and 5 wt.% of CNT to prepare filaments. The elastic modulus of PLA increased by 30% when 5 wt.% CNT was added, but toughness and tensile strength decreased by 22 and 11%, respectively. Magri et al. [19] studied the effect of infill line orientations and nozzle temperature on short carbon fiber (CF) reinforced PLA parts. They found that PLA/CF composite samples had better tensile properties than pure PLA samples because of the strengthening effect of high modulus CFs. Moreover, it was observed that the orientation of the infill line orientations and temperature of the nozzle were important factors in the mechanical properties of the PLA/CF composite parts printed by FFF method. Mihankhah et al. [20] investigated the mechanical properties of PLA/nanoclay printed parts. For this purpose, nanoclay content (0, 2 and 4 wt.%), nozzle temperature (190, 210 and 230 °C) and raster angle (0, 45 and 90 °) were considered as input variables and tensile strength as output variable. By adding 2 and 4 wt.% of nanoclay, tensile strength was enhanced by 4.6% and 15.3%, respectively. The optimal conditions were determined to be 4 wt.% of nanoclay, 230 °C nozzle temperature, and 0° raster angle.

It is evident from the above literature that several parameters in the FFF process can have a significant impact on the printed parts properties and quality, for example, nozzle temperature, infill density (percentage), infill pattern, layer thickness, printing speed, etc. [21]. Consequently, it is necessary to investigate the influence of process parameters of the FFF method on the properties of printed parts, but many experiments are required to investigate and optimize the required procedure. An increase in the number of experiments leads to an increase in the cost, time, and materials consumed in each experiment, which can be overcame by using design of experiments (DOE) [22-24]. It is widely accepted that one of the most common and practical DOE

methods for optimization, especially in engineering problems, is the response surface method (RSM). It is a method for modeling and analyzing a process in which the response of interest is affected by various variables, the purpose of which is to optimize the response. It is capable to evaluate the effects of multiple factors and their interactions on one or more response variables. In addition to mathematical modeling of the system, RSM saves time and cost by reducing the number of experiments [25-27].

Through an extensive literature review, it was found that various studies have been conducted to investigate the mechanical properties of PLA composites produced by FFF 3D printers. However, to the best of our knowledge, no prior research has focused on optimizing the printing parameters that affect the impact strength and specific impact strength of PLA/iron composites printed using FFF technology. Therefore, this study aimed to fill this research gap by conducting a simultaneous investigation of the effects of three printing parameters, namely printing speed, nominal porosity, and nozzle temperature, on two response variables, namely impact strength and specific impact strength. Additionally, the study utilized the RSM technique to determine the optimal combination of these parameters for improving the properties of PLA/iron composites. This contribution was significant in two ways: First, simultaneously investigation the effects of three printing parameters on response variables; and second, the RSM technique was used to examine the relationship between printing parameters and responses to determine the optimum combination of these parameters n the properties of PLA/iron composites.

2. Experimental procedure

2.1. Material and parts fabrication

The filament used in this study was a PLA/iron filament produced by Proto-Pasta, USA, with a diameter of 1.75 mm and an iron content of 45% by volume. The maximum particle size of the iron powder was 250 µm, and the filament density was 1.85 gr/cm^3. Prior to printing, the filament was dried for 6 hours at 60 °C. PLA/iron samples were designed based on the ASTM D6110 standard using SOLIDWORKS 2016 modeling software as shown in Figure 1. The model designed in the SLDPRT format was later converted to STL format after it had been designed, in order to use it in the PrusaSlicer software. By using this software, the CAD model can be sliced into layers, process parameters can be customized, and G-code can be generated. In order to print the samples, the prepared G-code file was imported into a Creality Ender-3 V2 machine. There are several 3D printer parameters that must be defined and set constant in order to stabilize the printing process and prevent extensive changes during the printing process. Aside from the printing speed, infill percentage and nozzle temperature that are the input variables, all other parameters were kept constant. Table 1 indicates the 3D printer parameters that were kept constant during this study.

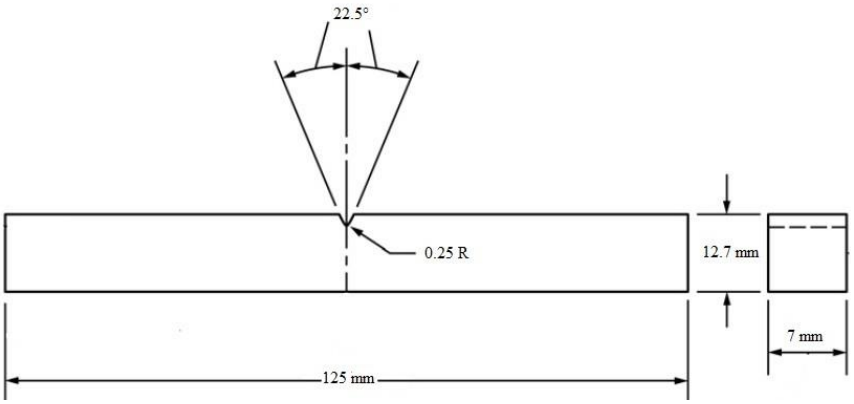

Figure 1. Sample geometry according to ASTM D6110

Table 1. Constant parameters during the FFF process

Parameters	Constant values	Units
Layer thickness	0.2	mm
First layer thickness	0.15	mm
Vertical Shell	2	Wall
Horizontal Shell: Solid layer	Top and bottom: 2	Layer
Infill pattern	Rectilinear	-
Top and bottom infill pattern	Rectilinear	-
Raster angle	-45/+45	°
Extrusion width	0.45	mm
Bed temperature	60	°C
Nozzle diameter	0.4	mm

2.2. Characterization methods

Impact test measures the materials resistance to failure owing to a suddenly applied force. An impact test of a material can be conducted in two ways, using Charpy and Izod impact tests. A swinging pendulum is used in both tests to strike a notched sample. A fundamental difference between the Izod impact test and the Charpy impact test is the orientation of the sample. During the Izod impact test, the sample is held vertically with the notch facing the pendulum, while during the Charpy impact test, the sample is held horizontally with the notch facing away from the pendulum [28]. In this study, the Charpy impact test machine of Novavaran Baspar Co. was used to evaluate the impact resistance of printed PLA/iron samples. The impact strength was calculated by dividing the absorbed energy before the failure by the cross-section area of the sample in the failure location. In order to calculate the absorbed energy, the following formula was used [29]:

$$Energy = P.L.(cos\alpha_2 - cos\alpha_1) \quad (1)$$

where P is the weight of the pendulum hammer, L is the hammer length, α_1 and α_2 are the initial and final angles, respectively. The weight of the pendulum was 2.036 kg, the length from the axis to the percussion center was 0.3948 m, and the initial angle was 150°. Also, the specific impact strength was also evaluated as the ratio of the impact strength of the sample to the density of the

sample. The water displacement method based on the ASTM D792 standard was used to measure the density of the samples. FX300GD (A&D Co, Japan) digital balance was used for this measurement.

A DMI Victory inverted metallographic microscope, model Dewinter (New Delhi, India) was also used to evaluate the structural properties of the printed samples.

2.3. Design of experiments

One of the most important methods for examining how process factors affect particular features is DOE. One of the DOE techniques that has fewer trials and, hence, less complexity than other strategies are the Box Behnken design (BBD) of RSM. This approach has three levels including -1, 0, +1 to divide design points related to input factors or parameters, where levels -1 and +1 are the minimum and maximum values of each input parameter, respectively, and level 0 is the average value of that parameter [30-32]. In 3D printing, printing speed, nozzle temperature and nominal porosity are critical parameters that directly affect the quality, strength, and appearance of the printed object. Printing speed, also known as print speed or feed rate, refers to how quickly the 3D printer's nozzle or print head moves while depositing material to create the layers of the 3D object. The nozzle temperature in 3D printing refers to the temperature of the hot end of the 3D printer's extruder nozzle, which melts and extrudes the thermoplastic material (usually filament) onto the build platform. This temperature is a crucial parameter because different materials have specific temperature requirements for proper extrusion. Nominal porosity denotes the percentage of void spaces within a printed object's internal structure, representing its level of porosity or solidity. This parameter is intimately linked to infill density, expressed as a percentage, which measures the volume of material filling the object's interior. Higher infill density equates to denser structures

with fewer voids, while lower percentages indicate increased porosity due to more internal empty spaces. Most 3D printing software allows users to adjust infill settings. By changing the infill density and infill pattern, can control the amount of material used and, consequently, the level of porosity in the final object. In this research, using the BBD approach and with the help of Minitab 21 software, the effects of printing speed, nominal porosity and nozzle temperature on the results of impact strength (IS) and specific impact strength (SIS) of printed samples constructed of PLA/iron composite in the FFF process are investigated. Elevating the printing temperature enhances layer adhesion, resulting in more robust components, yet excessively high temperatures can lead to defects like oozing, stringing, and warping. Conversely, reducing the temperature diminishes layer adhesion and structural integrity, potentially causing incomplete prints. Adjusting the printing speed can expedite the printing process, albeit at the cost of print quality, as it may introduce issues such as ringing, ghosting, and missed steps in the printer. Slower printing speeds yield superior quality but extend production times. Higher porosity means that there are more gaps or voids within the printed object. This can be intentional for certain applications where lightweight or porous structures are desired. However, high porosity can reduce the structural integrity and strength of the part. Lower porosity means that the printed object is more solid and dense. This is generally preferred for functional parts where strength and airtightness are crucial. However, it can result in heavier and less lightweight structures. The specific impact of these parameters hinges on 3D printing technology, material selection, and design, necessitating precise parameter optimization through experimentation for each project to attain the desired print quality and functionality. Thus, optimizing these parameters was the main goal. Three levels were taken into account for each of the input parameters. The process parameters of the variable levels are shown in Table 2.

Table 2. Input parameters and their variable levels

Process Parameters	Symbols	Units	Variable ranges		
			-1	0	+1
Printing speed	PS	mm/s	30	40	50
Nominal porosity	POR	%	30	50	70
Nozzle temperature	NT	°C	190	200	210

By using the levels of considered parameters, the test design table was created by BBD, which included 15 tests. Then, three impact test samples were printed for each test. Table 3 depicts the experimental designs and test results. Figure 2 depicts the printed impact test samples for the experimental design.

Table 3. Experimental design and output data

Experimentations order		Process parameter			Responses	
StdOrder	RunOrder	PS (mm/s)	POR (%)	NT (°C)	Impact strength (kJ/m^2)	Specific impact strength (J.m/kg)
13	1	40	50	200	2.089	1.808
7	2	30	50	210	2.967	2.454
8	3	50	50	210	2.746	2.297
1	4	30	30	200	2.746	1.886
5	5	30	50	190	2.300	2.154
11	6	40	30	210	2.970	2.649
9	7	40	30	190	3.871	2.727
14	8	40	50	200	2.089	1.840
10	9	40	70	190	1.874	1.731
2	10	50	30	200	3.415	2.438
12	11	40	70	210	2.080	1.809
6	12	50	50	190	2.970	2.562
4	13	50	70	200	1.659	1.284
3	14	30	70	200	1.874	1.811
15	15	40	50	200	2.092	1.844

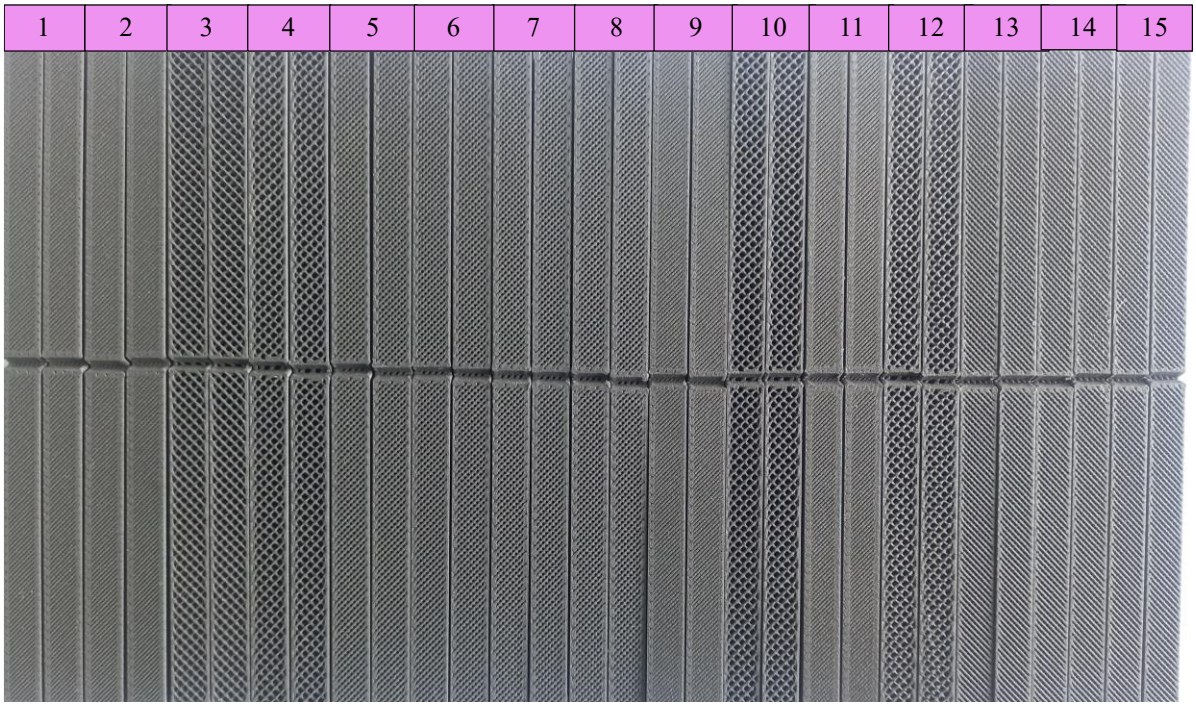

Figure 2. FFF PLA/iron samples (number coding and arrangement in accordance with RunOrder)

Another benefit of the RSM method is that it includes a regression model for predicting response variables. The RSM regression model is generally a quadratic full equation or a reduced form of it as Eq. (2) [33]:

$$y = \alpha_0 + \sum_{i=1}^{n} \alpha_1 x_i + \sum_{i=1}^{n} \alpha_2 x_i^2 + \sum_{i} \sum_{j} \alpha_3 x_i x_j + \varepsilon \quad (2)$$

where y is the measured response, α_0, α_1, α_2 and α_3 are constant, linear, quadratic and interaction coefficients, respectively. Also, $x_i$and x_j are the independent variables and ε is the experimental error. Based on the analysis of variance (ANOVA), the efficiency of the regression model is evaluated using R^2 as Eq. (3) [34]:

$$R^2 = 1 - \frac{ss_r}{ss_T} \quad (3)$$

where ss_r is the residual sum of squares and ss_T is the total sum of squares.

3. Results and discussion

Representative microscopic images of four samples have been presented in Figure 3. According to Table 3, the samples with 190 °C NT, 30% POR, and 40 mm/s PS and 200 °C NT, 30% POR, and 50 mm/s PS had the highest impact strength, with values of 3.871 and 3.415 kJ/m^2, respectively. The samples with 200 °C NT, 70% POR, and 50 mm/s PS and 200 °C NT, 70% POR, and 30 mm/s PS had the lowest impact strength, with values of 1.659 and 1.874 kJ/m^2, respectively. The microscopic structures of the four samples mentioned are visible in the Figure 3. Microscopic images revealed some intriguing findings, and it is evident from the images that the raster had good dimension stability for the samples with the highest impact strength while the raster displayed numerous dimensional changes for the samples with the lowest impact strength. Therefore, it can be inferred that varying FFF process parameter levels cause changes in the raster's dimensions, which in turn cause changes in impact properties.

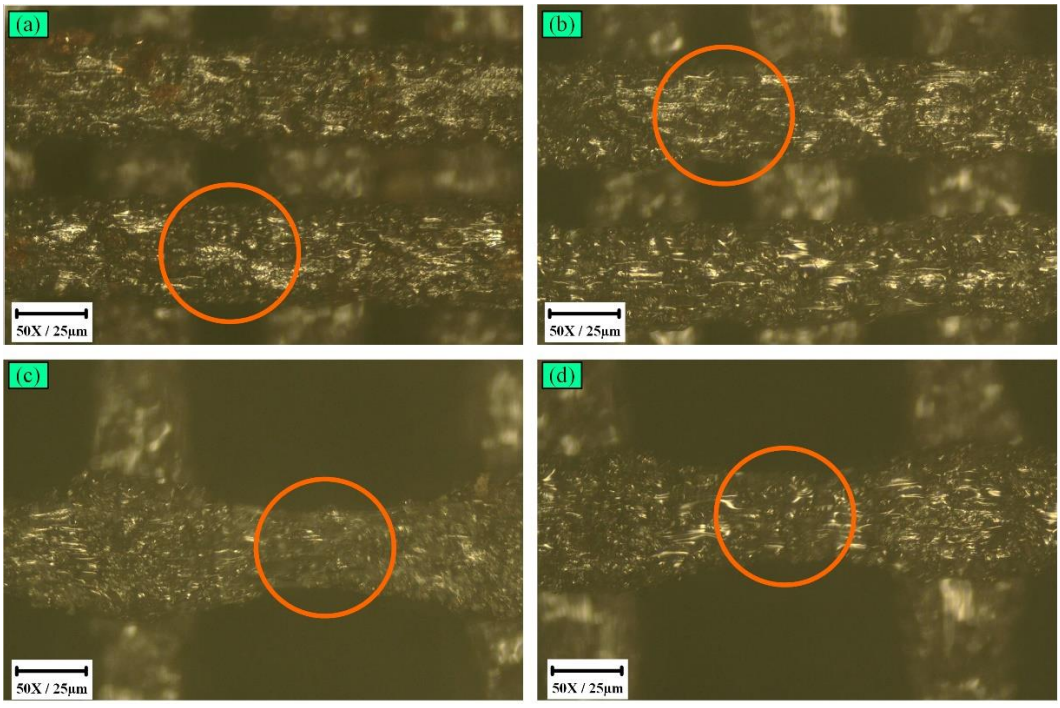

Figure 3. Representative microscopic images of impact strength samples a) 190 °C NT, 30% POR, and 40 mm/s PS, b) 200 °C NT, 30% POR, and 50 mm/s PS, c) 200 °C NT, 70% POR, and 50 mm/s PS and d) 200 °C NT, 70% POR, and 30 mm/s PS

3.1. Parametric study

Figure 4-a depicts the effects plot on IS. The graph illustrates that the highest IS value occurs when the nozzle temperature is almost 190 °C, the nominal porosity is 30% and the printing speed is 50 mm/s. From the effects plot shown in Figure 4-a, it is clear that the mean IS at the nozzle temperature of 190 °C is about 2.6 kJ/m^2 and at 200 and 210 °C, the IS is 2.1 and 2.5 kJ/m^2, respectively. From the result, it can be concluded that decreasing the nozzle temperature from 200 °C to 190 °C improves the IS by 23.8%. As nominal porosity increases from 30 to 70%, the IS decreases. This shows that with increase in nominal porosity, the IS of the printed parts is compromised. According to the effects plot in Figure 4-a, the mean IS at 30% of nominal porosity is 2.92 kJ/m^2, while at 50% and 70% of nominal porosity, the IS is 2.1 and 1.55 kJ/m^2, respectively. As a result, by reducing nominal porosity from 70% to 30%, 88.3% improvement is observed in the IS because when nominal porosity decreases, more material is deposited, and as nominal porosity decreases, the printed parts become more solid in structure. This observation is in accordance with the literature [29, 35]. Based on the effects plot, the mean IS at 30 mm/s is 2.18 kJ/m^2, while at 40 and 50 mm/s, the mean IS is 2.09 and 2.39 kJ/m^2, respectively. As a result, increasing printing speed from 30 to 40 mm/s results in 4.3% decrement in the IS, but increasing printing speed to 50 mm/s results in 14.35% improvement in the IS as compared to 40 mm/s of printing speed. At 30 mm/s, the slower printing speed allows for better layer bonding and improved interlayer adhesion. This leads to a sample with better IS. When the speed is increased to 40 mm/s, the reduced time for layers to bond properly can lead to a decrease in IS. However, when further increase the speed to 50 mm/s, it may encourage better interlayer bonding due to a combination of factors, such as improved melt flow. This improved bonding can enhance the IS compared to 40

mm/s. Similar outcomes and patterns have been attained for the SIS results, as shown in Figure 4-b. This confirms that the SIS is governed by the IS not the density.

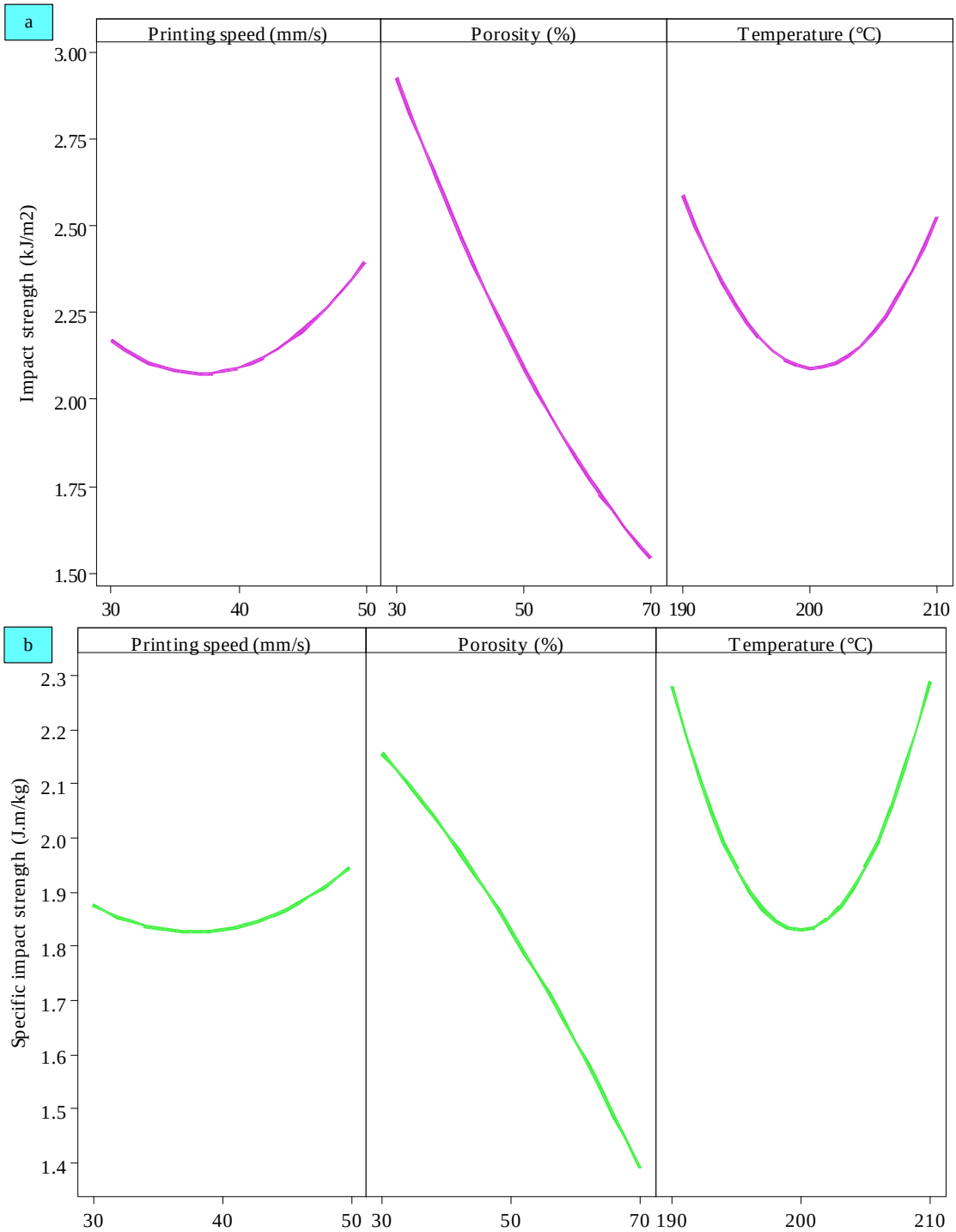

Figure 4. Effects of printing speed, nominal porosity, and temperature on (a) impact strength and (b) specific impact strength

3.2. ANOVA and RSM model fitting

ANOVA is used to examine how different response parameters are affected by process parameters (NT, POR, and PS). The parameters statistical significance is defined by the probability p-value, which should be less than the alpha value of 0.05 [36, 37]. In order to assess the performance of the models, ANOVA analysis was used to analyze the result of a full quadratic model and calculate their p-value and R-squared values. The main and interaction effects produced by the ANOVA are displayed in the Pareto charts. Additionally, they can recognize the standardized effects of the various NT, POR, and PS linear, quadratic, and interaction factors in comparison to the corresponding standard value of 2.57. In the model, any effects that are greater than this line (2.57) are deemed significant (see Figure 5) [38].

Figure 5-a shows the Pareto effects of impact strength with respect to processing parameters. The illustration shows that the nominal porosity has the most significant impact on impact strength with p-value of 0.000 (see Table 4), followed by the quadratic effects of nozzle temperature (NT*NT) and the NT*POR interaction, which have p-values of 0.005 and 0.030, respectively (see Table 4). The nozzle temperature, which has a p-value of 0.126, was the least important parameter in this predictive model. If the specific impact strength response is evaluated (Figure 5-b), it is clearly evident that the nominal porosity and the quadratic effects of nozzle temperature parameter (NT*NT) are significant with p-values of 0.000 (see Table 5). For specific impact strength response, as well as the impact strength chart, the nozzle temperature was the least significant parameter in this predictive model. The interactions of POR*PS and NT*PS are significant in the model with p-values of 0.003 and 0.041, respectively (see Table 5).

According to Table 4, the p-value of the model is 0.003, indicating that the model created for impact strength is statistically significant. The model is presented in Eq. (4):

$$IS = 187.9 - 1.845\,NT - 0.3028\,POR + 0.360\,PS + 0.004655\,NT * NT + 0.000358\,POR * POR + 0.001903\,PS * PS + 0.001384\,NT * POR - 0.002228\,NT * PS - 0.001105\,POR * PS \quad (4)$$

The R-sq parameter for the impact strength was equal to 97.02% according to the ANOVA results. This makes it clear that the generated regression model is effective enough to accurately forecast the impact strength.

Also, the model created for the specific impact strength has a p-value of 0.001, indicating that it is statistically significant, according to the results of the ANOVA in Table 5. The model is shown in Eq (5):

$$SIS = 173.5 - 1.774\,NT + 0.0100\,POR + 0.288\,PS + 0.004552\,NT * NT - 0.000142\,POR * POR + 0.000812\,PS * PS + 0.000195\,NT * POR - 0.001412\,NT * PS - 0.001350\,POR * PS \quad (5)$$

ANOVA result for the specific impact strength showed that R-sq parameter is equal to 97.79%. This clarifies that the obtained regression model is efficacious enough to predict the specific impact strength with satisfactory accuracy.

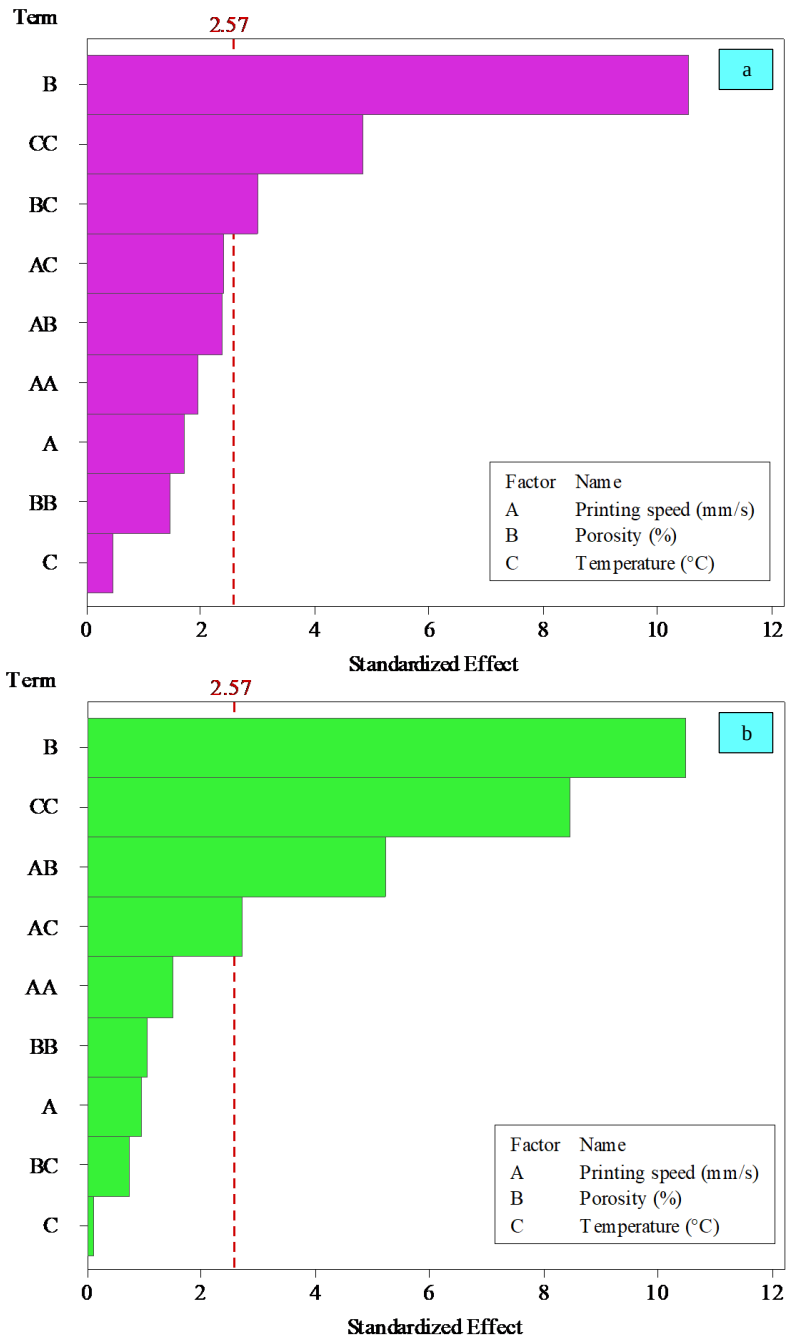

Figure 5. Pareto chart of the standardized effects of (a) impact strength (b) specific impact strength

Table 4. ANOVA analysis for the impact strength

Source	DF	Contribution	Adj SS	Adj MS	F-Value	P-Value
Model	9	97.02%	5.53535	0.61504	18.06	0.003
Linear	3	68.56%	3.91177	1.30392	38.29	0.001
NT (°C)	1	0.14%	0.00794	0.00794	0.23	0.650
POR (%)	1	66.63%	3.80190	3.80190	111.64	0.000
PS (mm/s)	1	1.79%	0.10193	0.10193	2.99	0.144

Square	3	16.18%	0.92338	0.30779	9.04	0.018
NT (°C)*NT (°C)	1	12.76%	0.80009	0.80009	23.49	0.005
POR (%)*POR (%)	1	1.08%	0.07577	0.07577	2.22	0.196
PS (mm/s)*PS (mm/s)	1	2.34%	0.13364	0.13364	3.92	0.104
2-Way Interaction	3	12.27%	0.70020	0.23340	6.85	0.032
NT (°C)*POR (%)	1	5.37%	0.30636	0.30636	9.00	0.030
NT (°C)*PS (mm/s)	1	3.48%	0.19847	0.19847	5.83	0.061
POR (%)*PS (mm/s)	1	3.42%	0.19536	0.19536	5.74	0.062
Error	5	2.98%	0.17027	0.03405	-	-
Lack-of-Fit	3	2.98%	0.17027	0.05676	18918.75	0.000
Pure Error	2	0.00%	0.00001	0.00000	-	-
Total	14	100.00%	5.70562	-	-	-
R-sq= 97.02%						

Table 5. ANOVA analysis for the specific impact strength

Source	DF	Contribution	Adj SS	Adj MS	F-Value	P-Value
Model	9	97.79%	2.36857	0.26317	24.61	0.001
Linear	3	48.90%	1.18432	0.39477	36.92	0.001
NT (°C)	1	0.01%	0.00015	0.00015	0.01	0.910
POR (%)	1	48.50%	1.17463	1.17463	109.86	0.000
PS (mm/s)	1	0.39%	0.00953	0.00953	0.89	0.388
Square	3	33.31%	0.80684	0.26895	25.15	0.002
NT (°C)*NT (°C)	1	31.69%	0.76501	0.76501	71.55	0.000
POR (%)*POR (%)	1	0.61%	0.01198	0.01198	1.12	0.338
PS (mm/s)*PS (mm/s)	1	1.01%	0.02437	0.02437	2.28	0.192
2-Way Interaction	3	15.58%	0.37741	0.12580	11.77	0.011
NT (°C)*POR (%)	1	0.25%	0.00610	0.00610	0.57	0.484
NT (°C)*PS (mm/s)	1	3.29%	0.07978	0.07978	7.46	0.041
POR (%)*PS (mm/s)	1	12.04%	0.29153	0.29153	27.27	0.003
Error	5	2.21%	0.05346	0.01069	-	-
Lack-of-Fit	3	2.17%	0.05267	0.01756	44.23	0.022
Pure Error	2	0.03%	0.00079	0.00040	-	-
Total	14	100.00%	2.42203	-	-	-
R-sq= 97.79%						

3.3. Single-objective optimization

Contour charts are useful for demonstrating the link between two independent variables and one dependent variable. These charts are based on the regression models. The response surface is represented in a contour plot as a two-dimensional plane where all points with the same response are joined to form contour lines with constant responses. Contour plot assists in understanding the nature of the link between the two inputs and the answer [38]. The single-objective optimization

results for the impact strength of PLA/iron composites printed samples are presented in Figure 6 regarding interaction effects of parameters. Figures 6-a shows that printing speed larger than 47 mm/s and nominal porosity less than 34% leads to the maximum impact strength which is larger than 3.2 kJ/m^2. According to the results of Figures 6-b, the largest impact strength, which are larger than 3 kJ/m^2, are obtained at the lowest nozzle temperatures and the highest printing speeds. Figures 6-c indicates that the maximum impact strength, which is larger than 3.5 kJ/m^2, is obtained at simultaneously the lowest levels of nozzle temperature and nominal porosity.

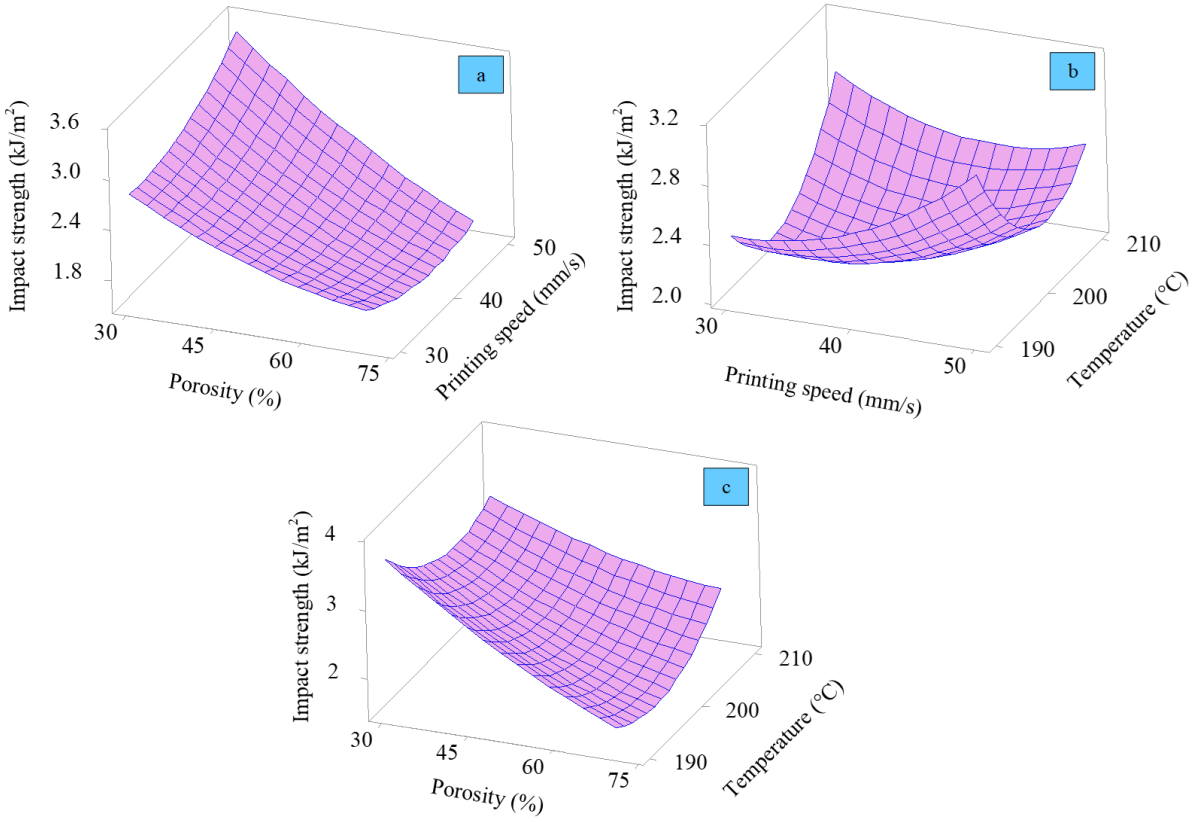

Figure 6. Single-objective optimization of impact strength of PLA/iron composites printed samples using surface plots; (a) POR vs PS, (b) NT vs PS, (c) NT vs POR

Figures 7 represents the single-objective optimization results for the specific impact strength of PLA/iron composites printed samples. Figures 7-a shows that the highest specific impact strength, which is greater than 2.4 J.m/kg, is obtained at printing speed greater than 47 mm/s and nominal

porosity less than 35%. Figures 7-b illuminates that the maximum specific impact strength which is larger than 2.5 J.m/kg is achieved at two different conditions of i) the highest printing speed and the lowest nozzle temperature and ii) the lowest printing speed and the highest nozzle temperature. Figures 7-c indicates that the maximum specific impact strength, which is larger than 2.5 J.m/kg, is obtained at two conditions of i) simultaneously lowest levels of nominal porosity and nozzle temperature and ii) the lowest levels of nominal porosity and the highest nozzle temperature.

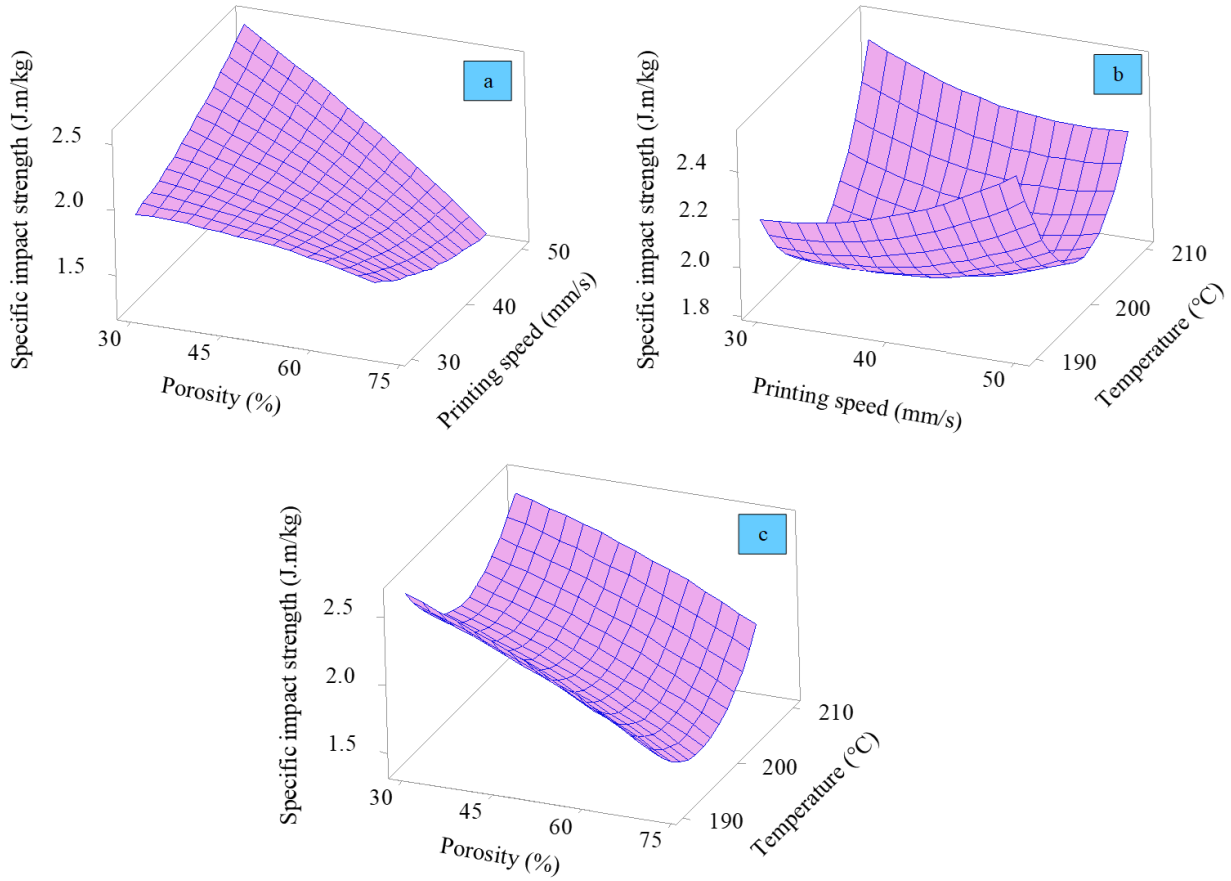

Figure 7. Single-objective optimization of specific impact strength of PLA/iron composites printed samples using surface plots; (a) POR vs PS, (b) NT vs PS, (c) NT vs POR

3.4. Multi-objective optimization results

The results of multi-objective optimization of impact strength and specific impact strength are presented in Table 6. The maximization of impact strength and specific impact strength were set

as the goals while printing speed (ranging from 30-50 mm/s), nozzle temperature (ranging from 190-210 °C) and nominal porosity (ranging from 30-70%) were considered as the variable parameters. According to the results of multi-objective optimization, the lowest level of nozzle temperature i.e. 190 °C, the lowest level of nominal porosity i.e. 30%, and the highest level of printing speed i.e. 50 mm/s are the multi-objective optimum conditions for achieving the maximum impact strength of 4.44 kJ/m^2 and the specific impact strength of 3.17 J.m/kg.

Table 6: Multi-objective optimization of impact strength and specific impact strength

Parameters	Range		Optimum level	Optimum response	
	Minimum	Maximum			
NT (°C)	190	210	190 °C	IS (kJ/m^2)	SIS (J.m/kg)
POR (%)	30	70	30%	4.44	3.17
PS (mm/s)	30	50	50 mm/s		

4. Conclusions

FFF 3D printing method for producing the PLA/iron samples was improved by response surface methodology approach and considering the significant input parameters (nozzle temperature, nominal porosity and printing speed) for each output parameter (the impact strength and specific impact strength). The following is a summary of the key findings. According to the Pareto effects, nominal porosity has the greatest effect on impact strength data, while nozzle temperature has the least effect. Decreasing the nominal porosity results in improving the impact strength of the samples. Nominal porosity and the second-order effects of the nozzle temperature parameter have a significant impact on the impact strength data, and like the impact strength results, the nozzle temperature shows the least effect on the specific impact strength data. The results related to multi-objective optimization also determine that the lowest level of nozzle temperature (190 °C), the

lowest level of nominal porosity (30%), and the printing speed of 50 mm/s are the multi-objective optimum conditions. At the optimum conditions, we achieve the maximum impact strength of 4.44 kJ/m^2 and the specific impact strength of 3.17 J.m/kg.

References

[1] Yang, Y., Dai, X., Yang, B., Zou, P., Gao, F., Duan, J. and Wang, C., 2023. Optimization of polylactic acid 3D printing parameters based on support vector regression and cuckoo search. *Polymer Engineering & Science*, https://doi.org/10.1002/pen.26440.

[2] Hasanzadeh, R., Mihankhah, P., Azdast, T., Aghaiee, S. and Park, C.B., 2023. Optimization of Process Parameters of Fused Filament Fabrication of Polylactic Acid Composites Reinforced by Aluminum Using Taguchi Approach. *Metals*, *13*(6), p.1013.

[3] Bikas, H., Stavropoulos, P. and Chryssolouris, G., 2016. Additive manufacturing methods and modelling approaches: a critical review. *The International Journal of Advanced Manufacturing Technology*, *83*(1), pp.389-405.

[4] Rasouli, A., Azdast, T., Mohammadzadeh, H., Mihankhah, P. and Hasanzadeh, R., 2021. Introducing a novel combined method of fused filament fabrication (FFF)/batch foaming to improve the properties of biodegradable poly lactic acid. *Modares Mechanical Engineering*, *22*(1), pp.15-22.

[5] Meiabadi, M.S., Moradi, M., Karamimoghadam, M., Ardabili, S., Bodaghi, M., Shokri, M. and Mosavi, A.H., 2021. Modeling the producibility of 3D printing in polylactic acid using artificial neural networks and fused filament fabrication. *Polymers*, *13*(19), 3219.

[6] Azdast, T. and Hasanzadeh, R., 2021. Polylactide scaffold fabrication using a novel combination technique of fused deposition modeling and batch foaming: dimensional accuracy and structural properties. *The International Journal of Advanced Manufacturing Technology*, *114*(5), pp.1309-1321.

[7] Tümer, E.H. and Erbil, H.Y., 2021. Extrusion-Based 3D printing applications of PLA composites: a review. *Coatings*, *11*(4), 390.

[8] Long, H., Wu, Z., Dong, Q., Shen, Y., Zhou, W., Luo, Y., Zhang, C. and Dong, X., 2019. Mechanical and thermal properties of bamboo fiber reinforced polypropylene/polylactic acid composites for 3D printing. *Polymer Engineering & Science*, *59*, pp.247-260.

[9] Hasanzadeh, R., Mihankhah, P., Azdast, T., Rasouli, A., Shamkhali, M. and Park, C.B., 2023. Biocompatible tissue-engineered scaffold polymers for 3D printing and its application for 4D printing. *Chemical Engineering Journal*, p.146616.

[10] Saini, P., Arora, M. and Kumar, M.R., 2016. Poly (lactic acid) blends in biomedical applications. *Advanced Drug Delivery Reviews*, *107*, pp.47-59.

[11] Banjanin, B., Vladić, G., Adamović, S. and Bošnjaković, G., 2022. Global market structure. In *Polymers for 3D Printing* (pp. 353-367). William Andrew Publishing.

[12] Kottasamy, A., Samykano, M., Kadirgama, K., Rahman, M. and Noor, M.M., 2022. Experimental investigation and prediction model for mechanical properties of copper-reinforced polylactic acid composites (Cu-PLA) using FDM-based 3D printing technique. *The International Journal of Advanced Manufacturing Technology*, *119*(7), pp.5211-5232.

[13] Zhang, X., Chen, L., Mulholland, T. and Osswald, T.A., 2019. Characterization of mechanical properties and fracture mode of PLA and copper/PLA composite part manufactured by fused deposition modeling. *SN Applied Sciences*, *1*(6), pp.1-12.

[14] Liu, Z., Lei, Q. and Xing, S., 2019. Mechanical characteristics of wood, ceramic, metal and carbon fiber-based PLA composites fabricated by FDM. *Journal of Materials Research and Technology*, *8*(5), pp.3741-3751.

[15] Hanon, M.M., Alshammas, Y. and Zsidai, L., 2020. Effect of print orientation and bronze existence on tribological and mechanical properties of 3D-printed bronze/PLA composite. *The International Journal of Advanced Manufacturing Technology*, *108*(1), pp.553-570.

[16] Selvamani, S.K., Rajan, K., Samykano, M., Kumar, R.R., Kadirgama, K. and Mohan, R.V., 2022. Investigation of tensile properties of PLA–brass composite using FDM. *Progress in Additive Manufacturing*, pp.1-13.

[17] Vinay, D.L., Keshavamurthy, R. and Tambrallimath, V., 2022. Enhanced Mechanical Properties of Metal filled 3D Printed Polymer Composites. *Journal of The Institution of Engineers (India): Series D*, pp.1-15.

[18] Patanwala, H.S., Hong, D., Vora, S.R., Bognet, B. and Ma, A.W., 2018. The microstructure and mechanical properties of 3D printed carbon nanotube-polylactic acid composites. *Polymer Composites*, *39*(S2), pp.1060-1071.

[19] Magri, A.E., El Mabrouk, K., Vaudreuil, S. and Touhami, M.E., 2021. Mechanical properties of CF-reinforced PLA parts manufactured by fused deposition modeling. *Journal of Thermoplastic Composite Materials*, *34*(5), pp.581-595.

[20] Mihankhah, P., Azdast, T., Mohammadzadeh, H., Hasanzadeh, R. and Aghaiee, S., 2021. Fused filament fabrication of biodegradable polylactic acid reinforced by nanoclay as a potential biomedical material. *Journal of Thermoplastic Composite Materials*, p.08927057211044185.

[21] Gonabadi, H., Yadav, A. and Bull, S.J., 2020. The effect of processing parameters on the mechanical characteristics of PLA produced by a 3D FFF printer. *The International Journal of Advanced Manufacturing Technology*, *111*(3), pp.695-709.

[22] Zhao, D., Zhou, R., Sun, J., Li, H. and Jin, Y., 2019. Experimental study of polymeric stent fabrication using homemade 3D printing system. *Polymer Engineering & Science*, *59*(6), pp.1122-1131.

[23] Hasanzadeh, R., Mojaver, P., Azdast, T., Khalilarya, S. and Chitsaz, A., 2023. Developing gasification process of polyethylene waste by utilization of response surface methodology as a machine learning technique and multi-objective optimizer approach. International Journal of Hydrogen Energy, 48(15), pp.5873-5886.

[24] Hasanzadeh, R., Mojaver, P., Chitsaz, A., Mojaver, M., Jalili, M. and Rosen, M.A., 2022. Biomass and low-density polyethylene waste composites gasification: Orthogonal array design of Taguchi technique for analysis and optimization. *International Journal of Hydrogen Energy*, *47*(67), pp.28819-28832.

[25] Xia, J., Liu, S., Zhang, B. and Chen, Y., 2021. Central Composite Experiment Design (CCD)-Response Surface Method (RSM) to Optimize the Sintering Process of Ti-6Al-4V Alloy. *Metals*, *11*(2), 197.

[26] Veza, I., Spraggon, M., Fattah, I.R. and Idris, M., 2023. Response surface methodology (RSM) for optimizing engine performance and emissions fueled with biofuel: Review of RSM for sustainability energy transition. *Results in Engineering*, p.101213.

[27] Moradi, M., Beygi, R., Amiri, A., da Silva, L.F.M. and Sharif, S., 2022. 3D Printing of Acrylonitrile Butadiene Styrene by Fused Deposition Modeling: Artificial Neural Network and Response Surface Method Analyses. *Journal of Materials Engineering and Performance*, pp.1-13.

[28] Kottasamy, A., Samykano, M., Kadirgama, K., Ramasamy, D., Rahman, M.M. and Pandey, A.K., 2021. Optimization of impact energy of copper-polylactic acid (cu-pla) composite using response surface methodology for fdm 3d printing. *Journal of Advanced Research in Fluid Mechanics and Thermal Sciences*, *84*(1), pp.78-90.

[29] Rasouli, A., Azdast, T., Mohammadzadeh, H., Mihankhah, P. and Hasanzadeh, R., 2022. Morphological properties and mechanical performance of polylactic acid scaffolds fabricated by a novel fused filament fabrication/gas foaming coupled method. *The International Journal of Advanced Manufacturing Technology*, *119*(11), pp.7463-7474.

[30] Vasanthi, P., Selvan, S.S., Devaraju, A. and Vijaya, B., 2022. Optimization of Nano Materials Using Response Surface Methodology. In *Recent Advances in Materials and Modern Manufacturing* (pp. 885-897). Springer, Singapore.

[31] Ribeiro, R., Romão, E.L., Luz, E., Gomes, J.H. and Costa, S., 2020. Optimization of the Resistance Spot Welding Process of 22MnB5-Galvannealed Steel Using Response Surface Methodology and Global Criterion Method Based on Principal Components Analysis. *Metals*, *10*(10), 1338.

[32] Kechagias, J.D. and Vidakis, N., 2022. Parametric optimization of material extrusion 3D printing process: an assessment of Box-Behnken vs. full-factorial experimental approach. *The International Journal of Advanced Manufacturing Technology*, *121*(5), pp.3163-3172

[33] Chelladurai, S.J.S., Murugan, K., Ray, A.P., Upadhyaya, M., Narasimharaj, V. and Gnanasekaran, S., 2021. Optimization of process parameters using response surface methodology: A review. *Materials Today: Proceedings*, *37*, pp.1301-1304.

[34] Mojaver, P., Hasanzadeh, R., Chitsaz, A., Azdast, T. and Mojaver, M., 2022. Tri-objective central composite design optimization of co-gasification of eucalyptus biomass and polypropylene waste. *Biomass Conversion and Biorefinery*, pp.1-13.

[35] El Magri, A. and Vaudreuil, S., 2021. Optimizing the mechanical properties of 3D-printed PLA-graphene composite using response surface methodology. *Archives of Materials Science and Engineering*, *112*, pp.13-22.

[36] Yan, X., Wang, G., Ma, C., Li, J., Cheng, S., Yang, C. and Chen, L., 2021. Effects of pollutants in alkali/surfactant/polymer (ASP) flooding oilfield wastewater on membrane fouling in direct contact membrane distillation by response surface methodology. *Chemosphere*, *282*, 131130.

[37] Afshari, M., Bakhshi, S., Samadi, M.R. and Afshari, H., 2023. Optimizing the mechanical properties of TiO2/PA12 nano-composites fabricated by SLS 3D printing. *Polymer Engineering & Science*, *63*(1), pp.267-280.

[38] Antony, J.I.J.U., 2014. A systematic methodology for design of experiments. *Design of experiments for engineers and scientists*, *2*, pp.33-50.